university of groningen / faculty of science and engineering

GUSTO balloon mission: commissioning data of [CII] emission of Eta Carina 5

Bachelor's Project Thesis

Silke Oosterhof, s4889150, s.a.oosterhof@student.rug.nl
Supervisors: R.S. Shipmann

Abstract:

Context: GUSTO's main objective is to map the galactic plane for [CII], [NII] and [OI] by use of on-the-fly mapping. All observations are made in sequences. This paper looks at the [CII] data from the commissioning observations of the GUSTO balloon mission pointed towards the Eta Carina 5 region. Aims: The aim of the project is to explain how the observations were done for the highlighted sequences. Then, the emission spectra of [CII] will be analyzed and the resolved velocity of the gas cloud will be determined. Method: By calculating the antenna temperature from the data, the emission spectra will be plotted. From here, the emission spectra will be studied. The flow of the observations will be found by making an overview of how the sequences were made. Results: The flow of the observations of sequences 00050 and 00051 was different. Where sequence 00050 had one source location, sequence 00051 had nine source locations. This made the calculation and analysis different for both sequences. In the anaylsis we find that both sequences show signs of CII emission and self-absorption. Conclusions: During the commissioning period of the GUSTO mission, the coordinates of the star finder were not yet correctly coupled with the coordinates in the data file. Given the incorrect coordinates, it is not exactly known where the CII emission and absorption are seen. We do see that the flow of the observation differs per sequence. From the nine points in sequence 00051, we can create a picture of the movements of the observed object and find that most of the emission is found for $l > 287.628\,\text{deg}$ and $b > 0.187$. In addition, for $l < 287.628\,\text{deg}$ and $b < 0.187$ we see more self-absorption with higher antenna temperatures.

1 Introduction

1.1 CII, NII and OI

The GUSTO balloon mission aimed to detect [CII], [NII], and [OI] in the galactic plane of the Milky Way and the Large Magellanic Cloud (LMC). Using its Terahertz heterodyne receiver, the telescope detects the fine-structure frequencies of [CII], [NII], and [OI] which are 1.9 THz, 1.46 THz and 4.7 THz respectively. These particles can give inside details of the properties and the distribution of particles of the interstellar medium (ISM) of the Milky Way. CII and OI produce one of the brightest emission lines in the Far nfrared spectrum in the Milky Way and are therefore good elements to use for tracing. Because [CII] has a lower ionization energy than hydrogen, it can trace regions with neutral hydrogen, as well as regions with ionized hydrogen and molecular hydrogen. CII can be found in photon dissociation regions, where HII and HI regions border each other (Seo, Goldsmith, et al., 2019). Moreover, [OI] lines are important coolants of the ISM together with [CII] and are a trace for star formation. Therefore, they are have an important role in the ISM for maintaining the energetic balance (Contursi, Baker, et al., 2017, Röllig, Ossenkopf, et al., 2006).

The detection of [NII] is more difficult, as it has a weaker emission line. Nitrogen has a potential energy higher than that of hydrogen, so ionized nitrogen can be found in HII regions. Therefore, by mapping [NII], [CII], and [OI], a detailed understanding of the ISM of the Milky Way can be made (Langer, Goldsmith, and Pineda, 2016).

1.2 GUSTO mission

The GUSTO, Galactic/Extragalactic ULDB Spectroscopic Terahertz Observatory, balloon mission from 2024 was set to map the Milky Way and the Large Magellanic Cloud (LMC) for [CII], [NII], and [OI] emission by using a Terahertz heterodyne receiver. The GUSTO telescope and instruments are provided by the University of Arizona, NASA's Jet Propulsion Laboratory, Massachusetts Institute of Technology, Arizona State University, and SRON Netherlands Institute for Space Research (NASA,

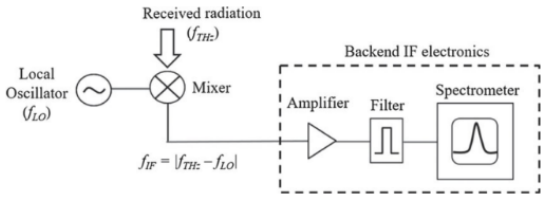

Figure 1.1: Schematic drawing of a heterodyne receiver system, including the local oscillator, mixer, amplifier, filter and the spectrometer. (Lin and Jarrahi, 2020)

2025). Earlier missions performed with heterodyne receivers were SOFIA and COBE (Heyminck, Graf, et al., 2012, Langer, Goldsmith, and Pineda, 2016). Where COBE had an angular resolution of 7 deg and a spectral resolution of 3000 km/s, the GUSTO telescope has an angular resolution of 45" and a spacial resolution of < 1 km/s, 10^4 times better than COBE. In addition, the GUSTO telescope has a coverage of more than 60 sq. deg, 30 times more than SOFIA's 2 sq. deg. (Kulesa, 2025). The mission is expecting to give a promising data map of the dynamics of ISM. The scientific goals of this mission are to get a better understanding of the dynamics and gas flows of the Galactic Center, as well as understanding the structure of the ISM in the Milky Way and the LMC (Kulesa, 2025). (Kulesa, 2025).

1.3 GUSTO telescope

1.3.1 Heterodyne receivers

A heterodyne receiver consists of mixer arrays, a local oscillator and the backend with a spectrometer. Figure 1.1 shows a schematic drawing of a heterdyne receiver system.

GUSTO's heterodyne receiver uses a 3 x 8 mixer array to calibrate the difference between the frequency of the electromagnetic (EM) signal of the observed object and the local oscillator. Each array of 8 mixers is coupled to an element. The local oscillator has a specific frequency range, close to the specific frequency that is looked for in the observed object. In the case of GUSTO's telescope, these frequencies are 1.9 THz for [CII], 1.4 THz for [NII], 4.7 THz for [OI] (Goldsmith, Bernasconi, et al., 2019). The mixer then takes the difference between the signal from the local oscillator and the EM signal, resulting in an intermediate frequency (IF). This IF will be down converted from THz to GHz to be analyzed by the autocorrelation spectrometer.

This IF is used to compute the emission spectra and can be converted to velocity in a frame of Earth's local standard rest (V_{LSR}). This velocity-resolved emission line shows us how fast the gas

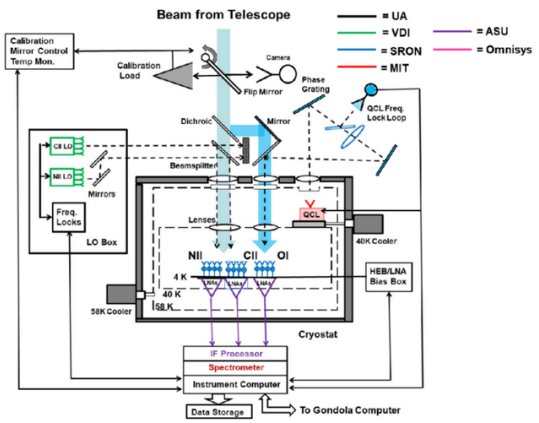

Figure 1.2: Schematic drawing of GUSTO's gondola. It shows the path of the incoming frequency beam (Walker, Kulesa, et al., 2022

cloud is moving. The Vlsr shows the movement of the object in the rest frame of the Earth.

Mixer 8 for [CII] is aligned with the telescope's boresight. This means that the coordinates for this mixer correspond to the coordinates that are given by the star finder. All other mixers have an offset to mixer 8. The offsets for all mixers are theoretically calculated. For mixer 5 of [CII], the offset is measured in the (Alt, Az) coordinates.

The mapping of [CII] and [NII] was possible, but the [OI] camera was not operational due to early on iceforming (SRON, 2024).

1.3.2 Sequences

The telescope observes an object in sequences, a calibratable series of scans that are used to calculate the antenna temperature. In this paper, sequences 00050 and 00051 are explored. Of a total of 12000 sequences, sequences 00050 and 00051 were made during the commissioning period. In these sequences, a multitude of scan types are performed. Scan types include a source scan(SRC), where the telescope first integrates over the object and then looks at a hot load (HOT) made possible by using a flip mirror. The same method is used to make a reference scan (REF). Here, the telescope is pointing towards a location that is known to have no emission of the preferred element. Then a scan of the hot load(REFHOT) is made again, using the flip mirror. In Figure 1.2, we see the path of an incoming frequency beam traveling through the telescope. Here, the flip mirror that is used for the hot load scans is shown. The main observations are made by on-the-fly mapping. On-the-fly mapping uses the telescope in a scanning motion, thus creating a scan of the galactic plane (National Radio Astronomy Observatory, 2025). This creates a complete map of the galactic plane for [CII] and [NII]. With the [CII] and [NII] being measured in

V_{LSR}, the dynamics of the ISM of the Milky Way can be computed, and a three dimensional map can be created.

1.4 Commissioning period

When the new telescope is made operational, a commissioning period must occur before the planned on-the-fly observations. In this first phase of the GUSTO mission, the telescope and all operations are checked and calibrations of all systems are done so that the telescope is working correctly and can be used for the planned observations. The main goal for the commissioning period is to collect emission data for all elements. For this to be achieved, an observation was done with the telescope pointing towards the Eta Carina 5 region. This region in the Milky Way is known to have PDR's and star formation clouds and therefore would be a good location for commissioning observations for [CII], [NII] and [OI](Seo, Goldsmith, et al., 2019).

The mixers that were found to be operational and gave readable emission spectra, were mixers 5 and 8 for [CII] and mixers 2, 3 and 6 for [NII]. The mixers for [OI] gave no readable signals. With mixer 8 of the CII camera being aligned with the boresight of the telescope, its coordinates can be used to determine the coordinates of the object that is observed. Mixer 5 of [CII] has a slight offset. The mixers for the [NII] observations are more offset from the boresight and are theoretically calculated.

1.5 In this paper

In this paper, we will look at two [CII] emission sequences from the commissioning period of the GUSTO balloon mission (2024). Looking at these data sequences we can find the flow of the observation and give information about the data set and the properties of the object that was observed. The mixers and sequences used for this paper are mixers 5 and 8, and sequences 00050 and 00051. In Section 2, the method for making the emission spectra will be briefly explained, and we will explore the information in the data file and find the flow of the observation. For Section 3, the emission spectra that were made for both the sequences and the mixers will be analyzed, as well as the properties of the emission lines. In Sections 4 and 5 we will discuss the results and give the conclusions found in this thesis.

2 Method

2.1 First plots

In the first stage, the first emission spectra were plotted for both sequences and mixers. It was assumed that the observations for both sequences were position switch observations for the same location. So, both sequences were expected to have one reference point and one source point. Using the data within the sequence data files, the antenna temperature can be calculated. The antenna temperature gives a measurement of the EM signals around the telescope. When the signal-to-noise ratio is high enough, the antenna temperature will result in readable emission spectra (Universidad Técnica Federico Santa María, 2025).

Using the source, reference, and hot loads data, the antenna temperature was calculated using Formula 2.1 (Köppen, 2011). Here T_{hot} is the set temperature of the hot load, T is the sky temperature calculated for the line frequency of [CII], y is the ratio between the average of the reference and the average of its hot load scans.

$$T_{sys} = \frac{T_{hot} - T * y}{y - 1} \tag{2.1}$$

To calculate the antenna temperature, we used the calculated system temperature and the data from the source and reference scans (Formula 2.2). Here, T_A^* is the antenna temperature in Kelvin, x_{src} is the averaged data from the source scans, x_{hot} is the averaged data from the hot load that is coupled to the source data, x_{ref} is the averaged data from the reference scans.

$$T_A^* = T_{sys} \cdot \frac{x_{src} - \frac{x_{hot}}{y}}{x_{ref}} \tag{2.2}$$

In Figures 2.1 and 2.2 we see the [CII] emission spectra of the sequences 00050 and 00051 for mixers 5 and 8, respectively. These figures show the antenna temperature of the emission line, which gives an indication of the intensity of the CII emission, over an IF range with an extra axes showing the V_{LSR}. The conversion from the IF to the V_{LSR} was done with the use of Formulas 2.3 and 2.4.

IF_{vlsr0} is the IF chosen to represent V_{LSR} and is found in the header of the sequence files to be 1250 MHz for sequences 00050 and 00051. IF_{obs} will be the observed frequency, IF_{line} is the frequency of the transition line for [CII].

$$v = (\frac{IF_{vlsr0} - IF_{obs}}{freq_{line}}) \cdot c \tag{2.3}$$

The V_{LSR} of the observed gas cloud will be calculated using the V_{LSR} in the header, that is set for each observation. For sequences 00050 and 00051 this will be -24.0 km/s.

$$V_{LSR} = v + V_{LSR0} \tag{2.4}$$

In further figures, we used only the V_{LSR} axes for a more readable plot.

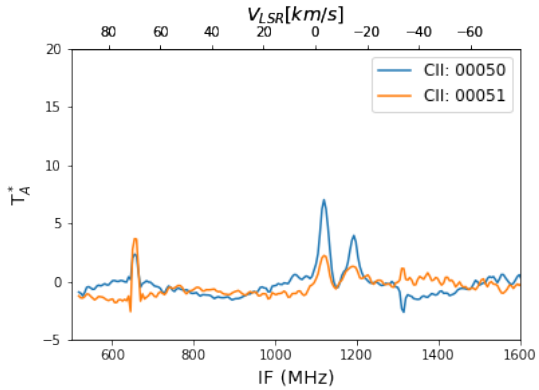

Figure 2.1: Figure of the [CII] emission spectra for sequences 00050 and 00051. Mixer 5.

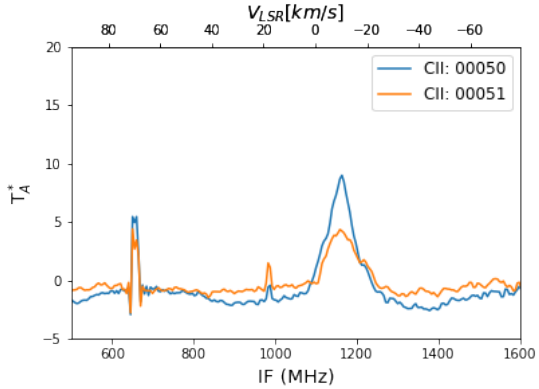

Figure 2.2: Figure of the [CII] emission spectra for sequences 00050 and 00051. Mixer 8.

When we focus on mixer 8, in Figure 2.2, we can see that both sequences show a peak. The frequency and velocity of the peaks are similar. The difference between the two sequences is its antenna temperature, and thus its intensity. The antenna temperature of sequence 00051 shows a spectrum that is significantly lower compared to sequence 00050. All emission spectra show a spur at a V_{LSR} of ~ 70 km/s (~ 650 MHz). This spur is the result of the collected data in the gondola being emitted back to the ground observatory. This creates a noise spur in the antenna temperature.

For the emission spectra of mixer 5 we observed the same lower antenna temperature for sequence 00051 (Figure 2.1). The emission spectra of mixer 5 give two smaller peaks, where the spectra in mixer 8 give one peak. This difference in the shape of the emission spectra is based on the offset in coordinate between mixer 5 and mixer 8. The emission spectra of mixer 5 therefore show a different part of the observed gas cloud. A more in-depth analysis of the emission spectra will be given in Section 3.

2.2 Comparison of the sequences

After concluding that the emission spectra for sequence 00051 showed a much lower antenna temperature compared to sequence 00050, a table was made for each sequence, as well as for each mixer (Tables A.2, A.3, A.4, A.5), to gain a better understanding of the way the observations were made. The information in the tables is similar for both mixers per sequence, except for the coordinates, which are different per mixer, due to the mixer offset. Therefore, when looking at the information within the tables, we will only look at the tables for mixer 8 (Tables A.3 and A.5). In these tables, the date, time, the scan types and coordinates of each scan in a sequence were made visible. A data log was made during the commissioning period to keep track of all observations made with the GUSTO telescope. When comparing the information in the data files with the relevant information in the data log containing the Eta Carina 5 observation (Table A.1) some inconsistencies were found in the date and coordinates. The date of the observation is not found on the data log; it is off by about an hour. This could be a human error, or it could be the result of the telescope moving through timezones during its flight. The other observation that could be made from the date column is that all dates and times are doubled, together with their fits file information (this is not represented in the tables to keep the tables clear, although this is visible in the original data files.). The reason for this is still unknown, although this occurs in all the data produced by the GUSTO balloon mission and will not be a problem with further calculations. For the inconsistent coordinates, we see that the galactic coordinates are significantly off. Where the data log stated a location of (l:287.6 and b: -0.3) and the data file stated a location of (l:287.6 and b:0.31 to 0.48). These coordinates in the data file are given for the boresight of the telescope, corresponding to the coordinates of mixer 8 for [CII]. The coordinates are shown in Figure 2.3. These regions are used by GUSTO during the commissioning period. The red box shows the coordinates for the source scans given in the data file. The blue dot represents the coordinates given in the data log. The red box is significantly off of the blue dot. From this figure, we also notice that the blue dot does not represent the Eta Carina 5 region, but rather the Eta Carina 3 region.

The reason for these inconsistencies for the coordinates is that the star finder on the telescope in these early stages of the mission was not yet correctly coupled with the coordinates that were put in the data file. Therefore, we should assume that the coordinates in the data log would be correct, assuming that the star finder itself was working correctly. Although we do not have all the coordinate

information available for all scans made during the observation in the data log, further calculations will still use the coordinates from the data file.

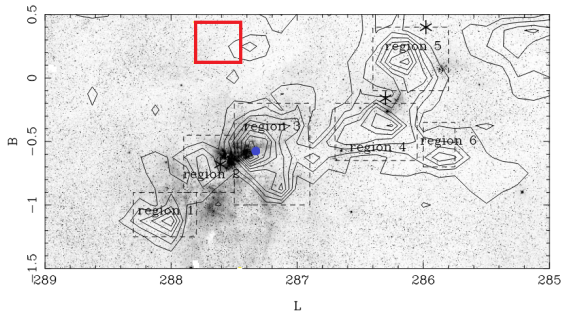

Figure 2.3: Map of the Carina molecular complex. The red box shows the coordinates given in the data file. The blue dot shows the coordinates given in the data log. Figure from Zhang, Lee, et al., 2001

2.3 Flow of the observation

Using Table A.3 , we found the order of the scans of the observation for sequence 00050. All scans are made in multitudes to increase the integration time. According to the scan types in the fits files, sequence 00050 starts with hot (REFHOT) and coupled reference (REF) scans. Then, two pairs of hot (HOT) and coupled source (SRC) scans were made. Then again a REFHOT and REF pair. Noticeable here are the coordinates at which the scans take place. The first pair of REFHOT and REF scans have the same coordinates as the HOT and SRC scans. These reference scans would not give the expected reference data. This could mean that there were mislabeled scans, and that the first pair of REFHOT and REF scans should be labeled as HOT and SRC respectively. With these observations, we dismiss the first REF and REFHOT, and this pair of REF and REFHOT scans will not be used in further calculations.

For sequence 00051 the course of the observation was notably different. Looking at Table A.5, the observation starts with the same pair of REFHOT and HOT scans. Then, there are nine pairs of HOT and SRC scans. Here, the pairs show nine different coordinates. This observation raised the question of what part of the sky was observed and how it was done. To give more insight in these questions, a plot was made showing all coordinates for both sequences 00050 and 00051. After plotting the coordinate points at which all scans were made, all points were visible on an grid of 8 by 8 arcminutes. Figure 2.4 shows the coordinate points for all source and reference scans of sequences 00050 and 00051, in addition to mixers 5 and 8. The blue and green crosses at the top of the figure represent the reference scans of mixers 5 and 8, respectively, for sequence 00050. The yellow and black dots represent the source and reference scans of mixers 5 and 8, respectively, for sequence 00051. The reference scans for sequence 00051 are not represented as different points because the coordinates of the reference scans for sequence 00051 overlay with the source scans at point 1. In Figure 2.4 we see for sequence 00050 that the source and reference points are well separated, and that there is only one source point. For sequence 00051 there are nine different source points. Here, the observation started at the center point and then spiraled outwards, visible by the numbering of the data points. All source points are separated by ~ 8 arcminutes. The reference point of sequence 00051 has the same location as the first source point of sequence 00051. We also notice that the starting point of the observations of sequence 00051, has the same location as the source point of sequence 00050. Using this point, we will compare both sequences in Figures 3.1 and 3.2.

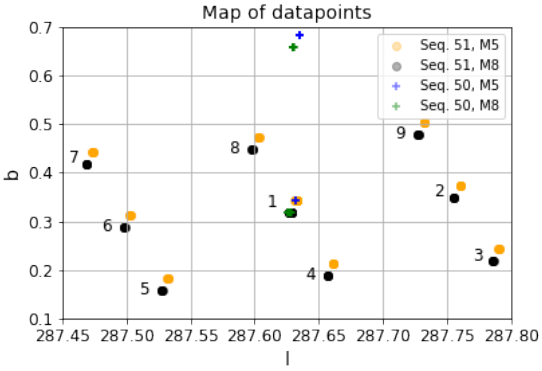

Figure 2.4: Map of the coordinates of all datapoints for sequence 00050 and sequence 00051.

Because the reference point of sequence 00051 can not be used as a reference scan, in further calculations, the reference scan of sequence 00050 will be used for the calculations with sequence 00051.

3 Analysis

To get an inside view on the properties of the gas cloud that was observed during the commissioning period, we analyzed the emission spectra for each mixer and sequence. The analysis is done for sequences 00050 and 00051 separately. The analysis of the emission spectra for both mixers will also be performed separately. This analysis of the line properties is estimated by eye, with an uncertainty of 1 K in antenna temperature and 1 km/s in V_{LSR}.

3.1 Sequence 00050

In Figures 3.1 and 3.2 we see the emission spectra of sequences 00050 and 00051 for both mixers at the coordinate point that they share. In these figures we see that the line shapes are similar for both sequences. Although the graph of sequence 00050 seems to have less noise present. This similarity shows that the calculations for the emission spectra are done correctly. Small differences between observations are always present.

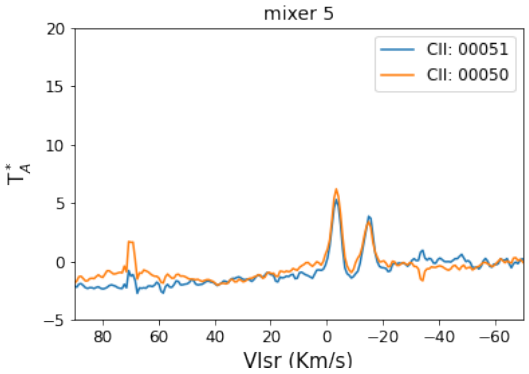

Figure 3.1: Figure of the [CII] emission spectra for point 1 of both sequence 00050 and 00051. Mixer 5.

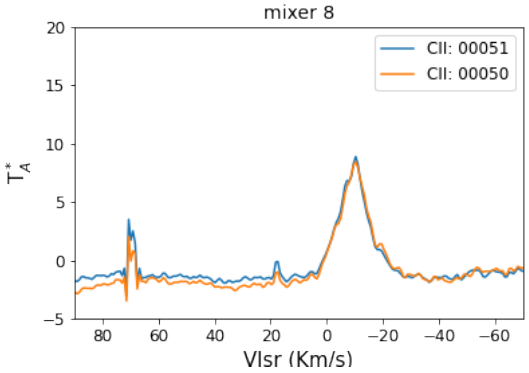

Figure 3.2: Figure of the [CII] emission spectra for point 1 of both sequence 00050 and 00051. Mixer 8.

Comparing Figures 3.1 and 3.2, we see the emission spectra of mixer 5 show two peaks where mixer 8 shows one clear peak, respectively. In Figure 3.1, the dip in the emission spectrum tells us that a part of the gas in the line of sight is optically thin and a part is optically thick (García, 2015). And so, the observed gas shows both emission lines and absorption lines. Combining the two peaks in a fitted graph, the velocity of the absorption line is similar to the to the velocity of the peak of the emission spectrum. Therefore, the gas cloud contains warmer and colder CII, respectively, and the emission spectrum shows self-absorption lines. In addition, we see that the emission line is shifted to the right and has a negative velocity. Resulting in the gas cloud moving towards the Earth. The estimated FWHM (Full Width Half Maximum) of the emission peak is ∼13 km/s. This broad line is the result of turbulence within the gas cloud, creating elements that move at different velocities. The estimated FWHM of the absorption peak is ∼6 km/s. The absorption line in the spectrum is the result of colder [CII] in the gas cloud. This colder gas has a lower temperature, and therefore the elements would move with a lower velocity. This is consistent with the estimated FWHM of the absorption line and the emission line.

The emission spectrum for mixer 8 shows a peak with an estimated FWHM of ∼11 km/s and an estimated antenna temperature of ∼9 K. The width of the peak tells us that the cloud contains elements that move faster and slower relative to each other. Whether this turbulence within the gas is the result of the cloud rotating or expanding cannot be determined with the information that is available. For this to be known, properties such as the critical density and the molecules' dipole moment are needed (García, 2015).

3.2 Sequence 00051

For sequence 00051 there are nine different spectra, one at each position. The spectra are labeled according to the order in which they were observed. These spectra for mixers 5 and 8 can be found in Figure 3.3 and 3.4, respectively. The reason for the difference in the flow of the observation could be to test the scanning function for the on-the-fly mapping. Although this is not explicitly mentioned in the data log.

For mixer 5 (Figure 3.3), we see for each spectrum an emission peak, with most of them also showing forms of absorption. The highest and broadest emission peaks are found at points 1, 2, and 9. In Figure 3.3 we see that the emission peaks are more shifted to lower velocities right panels, indicating that the gas cloud is moving faster towards us in the regions where $l > 287.628$ deg and $b > 0.187$ deg.

The same trends can be said for the spectra for mixer 8. We see in Figure 3.4 that the highest intensities can be seen at points 1, 2, 3, and 4. Although the absorption features are weaker in the spectra of mixer 8 compared to the spectra of mixer 5.

Similar emission spectra have been found for $CO(4 \rightarrow 3)$ emission around the Carina Nebula. Especially in regions 2 and 6 of the Carina Nebula Complex, double peaks were found similar to the double peaks at point 1 of mixer 5 (Figure 2.3). The V_{LSR} of the emission peaks found for CO in

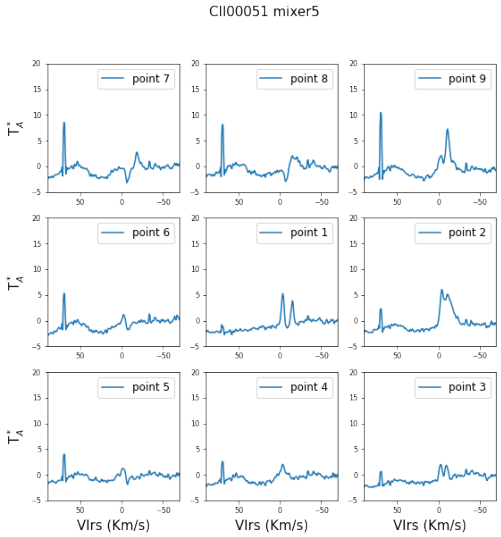

Figure 3.3: Figure of the [CII] emission spectra for each of the nine coordinates of the source points for sequence 00051. For mixer 5.

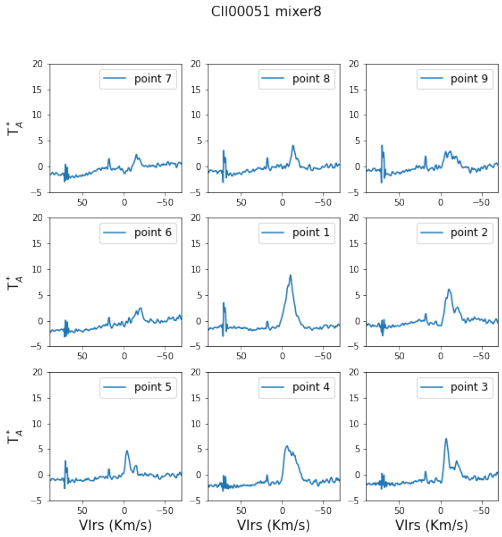

Figure 3.4: Figure of the [CII] emission spectra for each of the nine coordinates of the source points for sequence 00051. For mixer 8.

these regions are ~ -19 km/s to ~ -17 km/s. Furthermore, the CO in region 2 shows a peak V_{LSR} of ~ -25 km/s (Zhang, Lee, et al., 2001). The double peaks for CO were said to be the result of the interaction between the ambient gas and the winds and outflows coming from η Carina (Zhang, Lee, et al., 2001).

3.3 Line properties

For each emission line in the figures 3.3 and 3.4 the line properties are estimated. In Tables A.5 and A.6 a summary was made of peak T_A^*, peak velocity, peak FWHM, the absorption velocity and absorption FWHM.

The peak velocity values in the table for mixer 5 (A.6) tell something about the properties of the cloud that is observed. We can tell that the emission spectra in the center of the observed location, points 1,2 and 9, have the highest peak temperatures. This supports the observations in Figure 3.3. The lowest emission peak velocities are clearly visible at points 5 and 6. This is true for both mixers 5 and 8. The lowest values of the absorption velocities can be found at points 1 and 9 for mixer 8, and points 3 and 9 for mixer 5. The range of peak velocities is significant. These velocities range from -5 to -18 km/s. With the observed location, though unknown at which coordinates exactly, this range in velocities could still be assumed to be the same cloud, with the cloud being both optically thick and thin. This gives multiple layers within a cloud, where the center has a higher temperature, and therefore the gas is more turbulent.

Comparing the peak velocities of mixers 5 and 8, we see that they are closely similar with a few exceptions. Although the offset for mixer 5 is about ~ 1 arcminute, the separation between observation points is ~ 8 arcminute. Hence, the line shapes per coordinate point would be expected to have differences, where the line shapes for the two mixers would be expected to be more similar.

4 Discussion

In this paper we analyze two sequences of the commissioning data of the GUSTO balloon mission. When analyzing the sequence data files, there are inconsistencies found when comparing the information in the data log with the information in the data files.

First, the coordinates are off. When comparing the coordinates of the data log with the coordinates that were given, they are off by a degree for coordinate b.

Second, the star finder was not well connected to the location of the mixers and data files, and the offset of the star finder with the boresight was not yet calculated. This resulted in incorrect coordinates within the data files.

Furthermore, for better analysis of the emission spectra, Gaussian curves should be fitted to get more certain values for the line properties. The main goal of this thesis was to examine the data files for sequences 00050 and 00051, therefore, the emission line properties were not worked out in depth. In analyzing the emission spectra, we find multiple steep peaks at 70 km/s. These are interference peaks of the telescope when the data was

transmitted from the balloon to the Earth's surface observatory. These spurs should not be measured as emission lines.

Moreover, to gain further information about the properties of gas that was observed in these sequences, more spectra of other emission lines and elements are needed. For now we can not say for certain if this the [CII] resides from a PDR or HI/HII region. Further comparison of the [CII] lines with other observations of the Carina nebula complex is needed to say for certain that this is the correct location that was observed during the commissioning period.

5 Conclusions

The commissioning data from the GUSTO balloon mission of 2024, was found to contain some inconsistencies.

Comparing the data in the files of sequence 00050 and 00051 with the data in the data logs that were made during the observations, we found that some of the scan types were mislabeled, and that the coordinates in both the sequence files and the data log did not represent the object that was to be observed. The data log stated that the telescope was observing the Eta Carina 5 region, yet the coordinates in the data log represented the Carina nebula 3 region. Moreover, the coordinates in the sequence files showed a region that was off by a degree in galactic coordinate b.

Subsequently, when analyzing the flow of the observations for both sequence 00050 and 00051 there were also inconsistencies found. The course of the observations for sequence 00050 and sequence 00051 is fairly different. Where sequence 00050 was made with position switch observations, sequence 00051 made a 8 by 8 arcminute grid by taking nine source observations. This created a [CII] map of the grid, at location l: 287.469-287.86, b: 0.158-0.477. In addition, the reference scan for sequence 00051 was done at the same location as the first source scan of that sequence. Therefore, this reference scan can not be used as such, and the reference scan of sequence 00050 was used for all calculations of sequence 00050 and 00051.

Moreover, in the analysis of the observed gas cloud we found [CII] emission lines and [CII] absorption lines. This means, in addition with the broader line width that is found in the emission spectra, that the gas cloud contains hotter and colder ionized carbon, and that the cloud is somewhat turbulent. We also find that the gas cloud is moving faster towards the Earth in the regions where $l > 287.628$ deg and $b > 0.187$ deg. Stronger absorption lines are found in the opposite regions, where $l < 287.628$ deg and $b < 0.187$ deg. Altough some properties of the [CII] gas cloud were found in these commissioning data, we can not give an accurate conclusion on the properties of the gas cloud because the coordinates are inconsistent and the location of the observed gas cloud is not known.

References

Contursi, A., Baker, A. J., Berta, S., Magnelli, B., Lutz, D., Fischer, J., Verma, A., Nielbock, M., Grácia Carpio, J., Veilleux, S., Sturm, E., Davies, R., Genzel, R., Hailey-Dunsheath, S., Herrera-Camus, R., Janssen, A., Poglitsch, A., Sternberg, A., & Tacconi, L. J. (2017). Interstellar medium conditions in $z \tilde{} 0.2$ Lyman-break analogs. *Astronomy & Astrophysics*, *606*, A86. https://doi.org/10.1051/0004-6361/201730609

García, I. (2015). *Paving the path between low- and high-mass star formation.* [Master's thesis, Universiteit Leiden].

Goldsmith, P. F., Bernasconi, P. N., Walker, C. K., & KUlesa, C. (2019). The GUSTO balloon mission. Retrieved June 23, 2025, from https://ui.adsabs.harvard.edu/abs/2019AGUFM.A33Q2940B

Heyminck, S., Graf, U. U., Güsten, R., Stutzki, J., Hübers, H. W., & Hartogh, P. (2012). GREAT: The SOFIA high-frequency heterodyne instrument. *Astronomy & Astrophysics*, *542*, L1. https://doi.org/10.1051/0004-6361/201218811

Köppen, J. (2011). *Determine the System TEmperature.* https://portia.astrophysik.uni-kiel.de/~koeppen/Haystack/system.html

Kulesa, G. The 57-day stratospheric flight of gusto: Mapping [CII] and [NII] in the Milky Way and LMC. In: 2025.

Langer, W. D., Goldsmith, P. F., & Pineda, J. L. (2016). [C II] and [N II] from dense ionized regions in the Galaxy. *Astronomy & Astrophysics*, *590*, A43. https://doi.org/10.1051/0004-6361/201628151

Lin, Y.-J., & Jarrahi, M. (2020). Heterodyne terahertz detection through electronic and optoelectronic mixers. *Reports on Progress in Physics*, *83*(6), 066101. https://doi.org/10.1088/1361-6633/ab82f6

NASA. (2025). *GUSTO Overview.* https://science.nasa.gov/mission/gusto/

National Radio Astronomy Observatory. (2025). *On The Fly Mapping (OTF).* Retrieved June 25, 2025, from https://science.nrao.edu/facilities/vla/docs/manuals/opt-manual/observation-preparation-tool/scan-modes-obs-modes/on-the-fly-mosaicking

Röllig, M., Ossenkopf, V., Jeyakumar, S., Stutzki, J., & Sternberg, A. (2006). [CII] 158 m emission and metallicity in photon dominated regions. *Astronomy & Astrophysics*, *451*(3), 917–924. https://doi.org/10.1051/0004-6361:20053845

Seo, Y. M., Goldsmith, P. F., Walker, C. K., Hollenbach, D. J., Wolfire, M. G., Kulesa, C. A., Tolls, V., Bernasconi, P. N., Kavak, Ü., Van Der Tak, F. F. S., Shipman, R., Gao, J. R., Tielens, A., Burton, M. G., Yorke, H., Young, E., Peters, W. L., Young, A., Groppi, C., ... Kuiper, T. B. (2019). Probing ISM Structure in Trumpler 14 and Carina I Using the Stratospheric Terahertz Observatory 2. *The Astrophysical Journal*, *878*(2), 120. https://doi.org/10.3847/1538-4357/ab2043

SRON. (2024). *Active mission gusto*. https://www.sron.nl/en/missions/active/gusto/

Universidad Técnica Federico Santa María. (2025). *Lecture 7: Antenna Noise Temperature and System SIgnal-to-Noise Ratio*. http://www2.elo.utfsm.cl/~elo352/biblio/antenas/Lectura%207.pdf

Walker, C. K., Kulesa, C. A., Young, A., Verts, W., Gao, J.-R., Hu, Q., Silva, J. R., Mirzaei, B., Laauwen, W., Hesler, J. L., Groppi, C., & Emrich, A. (2022, August). Gal/xgal u/ldb spectroscopic/stratospheric thz observatory: Gusto. In J. Zmuidzinas & J.-R. Gao (Eds.), *Millimeter, submillimeter, and far-infrared detectors and instrumentation for astronomy xi* (p. 22). SPIE. https://doi.org/10.1117/12.2629051

Zhang, X., Lee, Y., Bolatto, A., & A., S. A. (2001). CO ($J = 4 > 3$) and [CI] observations of the carina molecular cloud complex. *THE ASTROPHYSICAL JOURNAL*.

A Appendix

Table A.1: Table of useful information from the data log.

Date	Time	Scan ID	Scan-type	Coordinates	Location
01-11-24	10:47:25	01457	SRC	(287.380, -0.640)	etaCar5
01-11-24	10:48:20	01459	REF	(287.380, -0.300)	etaCar5
01-11-24	10:48:48	01460	SRC	(287.380, -0.640)	etaCar5
01-11-24	10:49:30	01461	SRC	(287.380, -0.640)	etaCar5
01-11-24	10:50:01	01462	REF	(287.380, -0.300)	etaCar5
01-11-24	10:50:21	01463	REF	(287.380, -0.300)	etaCar5
01-11-24	10:50:49	01464	SRC	(287.380, -0.640)	etaCar5

Table A.2: Table of the information in the data file of sequence 00050, mixer 5. Highlighted rows show the mislabeled scans.

Date	Time	Scan-type	l	b
2024-01-11	11:48:24.794	REFHOT	287.632	0.343
2024-01-11	11:48:26.960	REFHOT	287.632	0.343
2024-01-11	11:48:29.127	REFHOT	287.632	0.343
2024-01-11	11:48:33.702	REF	287.632	0.343
2024-01-11	11:48:35.868	REF	287.632	0.343
2024-01-11	11:48:50.98	HOT	287.631	0.343
2024-01-11	11:48:53.148	HOT	287.631	0.343
2024-01-11	11:48:55.315	HOT	287.632	0.343
2024-01-11	11:49:00.188	SRC	287.631	0.343
2024-01-11	11:49:02.354	SRC	287.631	0.343
2024-01-11	11:49:04.521	SRC	287.631	0.343
2024-01-11	11:49:06.688	SRC	287.631	0.343
2024-01-11	11:49:32.365	HOT	287.632	0.343
2024-01-11	11:49:34.531	HOT	287.632	0.342
2024-01-11	11:49:36.698	HOT	287.633	0.342
2024-01-11	11:49:41.477	SRC	287.632	0.342
2024-01-11	11:49:43.643	SRC	287.632	0.342
2024-01-11	11:49:45.810	SRC	287.632	0.343
2024-01-11	11:49:47.977	SRC	287.632	0.343
2024-01-11	11:50:03.883	REFHOT	287.635	0.682
2024-01-11	11:50:06.049	REFHOT	287.635	0.682
2024-01-11	11:50:08.216	REFHOT	287.635	0.682
2024-01-11	11:50:12.870	REF	287.635	0.682
2024-01-11	11:50:15.036	REF	287.635	0.682
2024-01-11	11:50:17.203	REF	287.635	0.683
2024-01-11	11:50:19.370	REF	287.635	0.683

Table A.3: Table of the information in the data file of sequence 00050, mixer 8. Highlighted rows show the mislabeled scans.

Date	Time	Scan-type	l	b
2024-01-11	11:48:24.794	REFHOT	287.627	0.318
2024-01-11	11:48:26.960	REFHOT	287.627	0.318
2024-01-11	11:48:29.127	REFHOT	287.627	0.318
2024-01-11	11:48:33.702	REF	287.627	0.318
2024-01-11	11:48:35.868	REF	287.627	0.318

2024-01-11	11:48:50.982	HOT	287.626	0.318
2024-01-11	11:48:53.148	HOT	287.627	0.318
2024-01-11	11:48:55.315	HOT	287.627	0.318
2024-01-11	11:49:00.188	SRC	287.626	0.318
2024-01-11	11:49:02.354	SRC	287.626	0.318
2024-01-11	11:49:04.521	SRC	287.626	0.318
2024-01-11	11:49:06.688	SRC	287.626	0.317
2024-01-11	11:49:32.365	HOT	287.628	0.317
2024-01-11	11:49:34.531	HOT	287.627	0.317
2024-01-11	11:49:36.698	HOT	287.628	0.317
2024-01-11	11:49:41.477	SRC	287.628	0.317
2024-01-11	11:49:43.643	SRC	287.628	0.317
2024-01-11	11:49:45.810	SRC	287.627	0.317
2024-01-11	11:49:47.977	SRC	287.627	0.318
2024-01-11	11:50:03.883	REFHOT	287.63	0.656
2024-01-11	11:50:06.049	REFHOT	287.63	0.657
2024-01-11	11:50:08.216	REFHOT	287.63	0.657
2024-01-11	11:50:12.870	REF	287.63	0.657
2024-01-11	11:50:15.036	REF	287.63	0.657
2024-01-11	11:50:17.203	REF	287.63	0.657
2024-01-11	11:50:19.370	REF	287.63	0.657

Table A.4: Table of the information in the data file of sequence 00051, mixer 5.

Date	Time	Scan-type	l	b	Map point
2024-01-11	11:50:26.038	REFHOT	287.633	0.343	1
2024-01-11	11:50:28.204	REFHOT	287.633	0.343	1
2024-01-11	11:50:30.371	REFHOT	287.633	0.343	1
2024-01-11	11:50:34.940	REF	287.633	0.343	1
2024-01-11	11:50:37.106	REF	287.633	0.343	1
2024-01-11	11:50:51.822	HOT	287.633	0.342	1
2024-01-11	11:50:53.988	HOT	287.633	0.342	1
2024-01-11	11:50:56.155	HOT	287.633	0.343	1
2024-01-11	11:51:00.903	SRC	287.633	0.343	1
2024-01-11	11:51:03.069	SRC	287.633	0.343	1
2024-01-11	11:51:05.236	SRC	287.633	0.343	1
2024-01-11	11:51:07.403	SRC	287.633	0.343	1
2024-01-11	11:53:16.189	HOT	287.632	0.343	1
2024-01-11	11:53:19.189	HOT	287.632	0.343	1
2024-01-11	11:53:22.189	HOT	287.632	0.343	1
2024-01-11	11:53:27.685	SRC	287.631	0.343	1
2024-01-11	11:53:30.685	SRC	287.631	0.343	1
2024-01-11	11:53:43.820	HOT	287.76	0.373	2
2024-01-11	11:53:46.820	HOT	287.761	0.373	2
2024-01-11	11:53:49.820	HOT	287.76	0.373	2
2024-01-11	11:53:55.211	SRC	287.76	0.373	2
2024-01-11	11:53:58.211	SRC	287.76	0.373	2
2024-01-11	11:54:09.335	HOT	287.791	0.243	3
2024-01-11	11:54:12.335	HOT	287.791	0.244	3
2024-01-11	11:54:15.335	HOT	287.79	0.243	3
2024-01-11	11:54:20.720	SRC	287.791	0.244	3
2024-01-11	11:54:23.720	SRC	287.79	0.243	3
2024-01-11	11:54:35.376	HOT	287.661	0.213	4
2024-01-11	11:54:38.376	HOT	287.661	0.213	4
2024-01-11	11:54:41.376	HOT	287.661	0.213	4
2024-01-11	11:54:46.983	SRC	287.661	0.213	4
2024-01-11	11:54:49.983	SRC	287.661	0.213	4

2024-01-11	11:55:03.149	HOT	287.532	0.183	5
2024-01-11	11:55:06.149	HOT	287.533	0.183	5
2024-01-11	11:55:09.149	HOT	287.532	0.183	5
2024-01-11	11:55:14.855	SRC	287.532	0.183	5
2024-01-11	11:55:17.855	SRC	287.532	0.183	5
2024-01-11	11:55:28.387	HOT	287.502	0.313	6
2024-01-11	11:55:31.387	HOT	287.503	0.312	6
2024-01-11	11:55:34.387	HOT	287.503	0.313	6
2024-01-11	11:55:39.890	SRC	287.503	0.313	6
2024-01-11	11:55:42.890	SRC	287.503	0.312	6
2024-01-11	11:55:53.598	HOT	287.473	0.443	7
2024-01-11	11:55:56.598	HOT	287.473	0.443	7
2024-01-11	11:55:59.598	HOT	287.474	0.443	7
2024-01-11	11:56:05.000	SRC	287.474	0.443	7
2024-01-11	11:56:08.000	SRC	287.474	0.443	7
2024-01-11	11:56:20.343	HOT	287.603	0.473	8
2024-01-11	11:56:23.343	HOT	287.603	0.473	8
2024-01-11	11:56:26.343	HOT	287.603	0.472	8
2024-01-11	11:56:32.024	SRC	287.602	0.472	8
2024-01-11	11:56:35.024	SRC	287.604	0.472	8
2024-01-11	11:56:46.998	HOT	287.732	0.503	9
2024-01-11	11:56:49.998	HOT	287.732	0.503	9
2024-01-11	11:56:52.998	HOT	287.732	0.503	9
2024-01-11	11:56:58.600	SRC	287.733	0.503	9
2024-01-11	11:57:01.600	SRC	287.733	0.502	9

Table A.5: Table of the information in the data file of sequence 00051, mixer 8.

Date	Time	Scan-type	l	b	Map point
2024-01-11	11:50:26.038	REFHOT	287.633	0.317	1
2024-01-11	11:50:28.204	REFHOT	287.633	0.317	1
2024-01-11	11:50:30.371	REFHOT	287.633	0.317	1
2024-01-11	11:50:34.940	REF	287.633	0.317	1
2024-01-11	11:50:37.106	REF	287.633	0.317	1
2024-01-11	11:50:51.822	HOT	287.633	0.317	1
2024-01-11	11:50:53.988	HOT	287.633	0.317	1
2024-01-11	11:50:56.155	HOT	287.633	0.317	1
2024-01-11	11:51:00.903	SRC	287.633	0.317	1
2024-01-11	11:51:03.069	SRC	287.633	0.318	1
2024-01-11	11:51:05.236	SRC	287.633	0.318	1
2024-01-11	11:51:07.403	SRC	287.633	0.317	1
2024-01-11	11:53:16.189	HOT	287.632	0.318	1
2024-01-11	11:53:19.189	HOT	287.632	0.318	1
2024-01-11	11:53:22.189	HOT	287.632	0.317	1
2024-01-11	11:53:27.685	SRC	287.631	0.318	1
2024-01-11	11:53:30.685	SRC	287.631	0.318	1
2024-01-11	11:53:43.820	HOT	287.76	0.348	2
2024-01-11	11:53:46.820	HOT	287.761	0.348	2
2024-01-11	11:53:49.820	HOT	287.76	0.348	2
2024-01-11	11:53:55.211	SRC	287.76	0.348	2
2024-01-11	11:53:58.211	SRC	287.76	0.348	2
2024-01-11	11:54:09.335	HOT	287.791	0.218	3
2024-01-11	11:54:12.335	HOT	287.791	0.219	3
2024-01-11	11:54:15.335	HOT	287.79	0.218	3
2024-01-11	11:54:20.720	SRC	287.791	0.218	3
2024-01-11	11:54:23.720	SRC	287.79	0.218	3
2024-01-11	11:54:35.376	HOT	287.661	0.187	4

2024-01-11	11:54:38.376	HOT	287.661	0.188	4
2024-01-11	11:54:41.376	HOT	287.661	0.188	4
2024-01-11	11:54:46.983	SRC	287.661	0.188	4
2024-01-11	11:54:49.983	SRC	287.661	0.188	4
2024-01-11	11:55:03.149	HOT	287.532	0.158	5
2024-01-11	11:55:06.149	HOT	287.533	0.158	5
2024-01-11	11:55:09.149	HOT	287.532	0.158	5
2024-01-11	11:55:14.855	SRC	287.532	0.158	5
2024-01-11	11:55:17.855	SRC	287.532	0.158	5
2024-01-11	11:55:28.387	HOT	287.502	0.287	6
2024-01-11	11:55:31.387	HOT	287.503	0.287	6
2024-01-11	11:55:34.387	HOT	287.503	0.287	6
2024-01-11	11:55:39.890	SRC	287.503	0.287	6
2024-01-11	11:55:42.890	SRC	287.503	0.287	6
2024-01-11	11:55:53.598	HOT	287.473	0.417	7
2024-01-11	11:55:56.598	HOT	287.473	0.418	7
2024-01-11	11:55:59.598	HOT	287.474	0.417	7
2024-01-11	11:56:05.000	SRC	287.474	0.417	7
2024-01-11	11:56:08.000	SRC	287.474	0.417	7
2024-01-11	11:56:20.343	HOT	287.603	0.447	8
2024-01-11	11:56:23.343	HOT	287.603	0.447	8
2024-01-11	11:56:26.343	HOT	287.603	0.447	8
2024-01-11	11:56:32.024	SRC	287.602	0.447	8
2024-01-11	11:56:35.024	SRC	287.604	0.447	8
2024-01-11	11:56:46.998	HOT	287.732	0.477	9
2024-01-11	11:56:49.998	HOT	287.732	0.477	9
2024-01-11	11:56:52.998	HOT	287.732	0.477	9
2024-01-11	11:56:58.600	SRC	287.733	0.477	9
2024-01-11	11:57:01.600	SRC	287.733	0.477	9

Table A.6: Properties of the emission spectra, mixer 5.

Point	T_A^* (K)	V_{peak} (km/s)	Peak FWHM (km/s)	V_{absorb} (km/s)	Absorption FWHM (km/s)
1	9	-9	13	-8	6
2	8	-7	13	-7	3
3	4	-6	8	-6	4
4	2	-5	8	-7	3
5	1.2	-5	13	-7	3
6	2	-6	11	-8	6
7	3	-18	5	-7	5
8	2.5	-17	9	-7	5
9	8	-8	7	-6	4

Table A.7: Properties of the emission spectra, mixer 8.

Point	T_A^* (K)	V_{peak} (km/s)	Peak FWHM (km/s)	V_{absorb} (km/s)	Absorption FWHM (km/s)
1	9	-10	11	-8	2
2	7	-14	13	-17	2
3	9	-12	14	-16	6
4	6.5	-8	16	-10	5
5	5	-5	12	-10	3
6	3.5	-18	8	-17	1
7	3	-17	7	-16	1
8	4.5	-15	8	-16	2
9	4	-12	11	-8	1

Table A.8: Table with information about the coordinates given in Figure 2.4, mixer 5.

Point	Time	Coordinate (l,b)
1	11:50:51.822	(287.633, 0.343)
2	11:53:43.820	(287.76, 0.373)
3	11:54:09.335	(287.791, 0.243)
4	11:54:35.376	(287.661, 0.213)
5	11:55:03.149	(287.532, 0.183)
6	11:55:28.387	(287.502, 0.313)
7	11:55:53.598	(287.473, 0.433)
8	11:56:20.343	(287.603, 0.473)
9	11:56:46.998	(287.733, 0.503)

Table A.9: Table with information about the coordinates given in Figure 2.4, mixer 8.

Point	Time	Coordinate (l,b)
1	11:50:51.822	(287.628, 0.317)
2	11:53:43.820	(287.756, 0.348)
3	11:54:09.335	(287.86, 0.218)
4	11:54:35.376	(287.657, 0.187)
5	11:55:03.149	(287.528, 0.158)
6	11:55:28.387	(287.498, 0.288)
7	11:55:53.598	(287.469, 0.417)
8	11:56:20.343	(287.598, 0.447)
9	11:56:46.998	(287.727, 0.477)